INTERNATIONAL JOURNAL FOR NUMERICAL METHODS IN FLUIDS
Int. J. Numer. Meth. Fluids 2007; **53**:485–506
Published online 6 July 2006 in Wiley InterScience (www.interscience.wiley.com). DOI: 10.1002/fld.1291

Stability of convective flows in cavities: Solution of benchmark problems by a low-order finite volume method

Alexander Yu. Gelfgat*, †

School of Mechanical Engineering, Faculty of Engineering, Tel-Aviv University, Ramat Aviv, 69978, Israel

SUMMARY

A problem of stability of steady convective flows in rectangular cavities is revisited and studied by a second-order finite volume method. The study is motivated by further applications of the finite volume-based stability solver to more complicated applied problems, which needs an estimate of convergence of critical parameters. It is shown that for low-order methods the quantitatively correct stability results for the problems considered can be obtained only on grids having more than 100 nodes in the shortest direction, and that the results of calculations using uniform grids can be significantly improved by the Richardson's extrapolation. It is shown also that grid stretching can significantly improve the convergence, however sometimes can lead to its slowdown. It is argued that due to the sparseness of the Jacobian matrix and its large dimension it can be effective to combine Arnoldi iteration with direct sparse solvers instead of traditional Krylov-subspace-based iteration techniques. The same replacement in the Newton steady-state solver also yields a robust numerical process, however, it cannot be as effective as modern preconditioned Krylov-subspace-based iterative solvers. Copyright © 2006 John Wiley & Sons, Ltd.

Received 6 March 2006; Revised 2 May 2006; Accepted 2 May 2006

KEY WORDS: finite volume method; hydrodynamic stability; Newton iteration; Arnoldi iteration

1. INTRODUCTION

The present study is devoted to analysis of stability of steady buoyancy convection flows by a low-order finite volume method. We consider several benchmark problems, part of which are widely known, and another part is added here to complete the study. The motivation for this work is the necessity to perform the stability analysis for many applied problems, which cannot be treated by spectral of pseudospectral methods. Clearly, before complicated applied problems are considered

*Correspondence to: Alexander Yu. Gelfgat, School of Mechanical Engineering, Faculty of Engineering, Tel-Aviv University, Ramat Aviv, 69978, Israel.
†E-mail: gelfgat@eng.tau.ac.il

Contract/grant sponsor: German-Israeli Foundation; contract/grant number: 1-794-145.10/2004

one needs an estimation of convergence of critical parameters. This can be gained from the study of several benchmark problems, for which the accurate and validated data is already established.

It is well known that spectral and pseudospectral methods yield the most accurate solutions for benchmark problems considering flows in rectangular cavities, and especially instabilities of these flows. We can cite, for example, results of Botella and Peyret [1] for the lid-driven cavity, results of Le Quéré [2] for the test problem of convection of air in a square cavity [3], results of Le Quéré [4] and Pulicani *et al.* [5] for the benchmark on convection of a low Prandtl number fluid in a horizontally elongated cavity [6], and results of Xin and Le Quéré [7] on the recent benchmark of convection of air in a tall rectangular cavity [8]. Many benchmark-quality results were obtained also by Gelfgat and co-authors in References [9–13] using a global Galerkin method. However, these methods are restricted to simple geometries and because of this cannot be applied to many practically important problems. As an example one can mention problems of melt instabilities in bulk crystal growth processes, which was the motivation for the benchmark [6].

Here we apply the second-order finite volume method to several problems of buoyancy and thermocapillary convection in rectangular cavities. It is emphasized that the numerical technique briefly described below is not restricted to a certain class of problems and already was applied for stability studies in Reference [14] and floating zone [15] crystal growth configurations. The studies of this kind usually have two main bottlenecks. The first one is connected with the calculation of steady-state flows, whose stability is to be studied. The Jacobian-free [16–19] or other inexact [20–22] and exact [23–26] Newton methods combined with a Krylov-subspace-based iterative linear solver [27] usually are applied for this purpose. These solvers are very effective when relatively simple benchmark problems are considered, however fail to converge in more complicated cases. There were also some reports about possible loss of accuracy when Jacobian-free approach is applied (see, e.g. Reference [28]). Therefore in the present study we calculate the Jacobian matrix using the corresponding analytical evaluations, which follow from the discretized equations, as it was done in References [23–26]. We also argue that when very fine grids are used and due to the high level of the sparseness of the Jacobian matrix it is possible to replace iterative solvers by direct ones, which can be slower but do not have a problem of divergency.

The second bottleneck is connected with the eigenvalue problem of very large dimension, which must be solved for the study of linear stability of a steady flow. The usual approach here is the Arnoldi iteration method, which allows one to calculate only necessary part of the whole spectrum. The Arnoldi iteration also needs computation of the Krylov-subspace basis. An additional difficulty here is connected with the incompressible continuity equation, which does not contain the time derivative. The latter requires considering the eigenvalue problem in the shift-and-invert mode [29] or use of the Cayley transformation [24–26]. Consequently, the Krylov basis vectors are to be computed as solutions of a system of linear algebraic equations. Again, we argue here that instead of iterative solvers, which can diverge and be CPU-time consuming, it can be more effective to built an **LU**-decomposition of the matrix, so that the necessary amount of the Krylov basis vectors will be computed by the back substitution. It can be expected that the two back-substitution procedures needed to extricate a solution from the already computed **LU**-decomposition will be faster than an iterative solver. The crucial question is how effective the initial **LU**-decomposition can be computed.

The effectiveness of the application of the direct sparse matrix solvers described here is the consequence of the matrix sparseness, which follows from the low-order discretization method applied. As reported below, we were able to perform calculations of steady states and stability analysis on the grids consisting of 450^2 nodes. The only restriction for the further grid refinement

DOI: 10.1002/fld

is the computer memory consumed by a direct sparse matrix solver. The results reported here are obtained on an Itanium-2 workstation with 16 Gbytes memory.

The convergence studies reported below show that correct critical parameters can be calculated only on rather fine grids having more than 100 nodes in the shortest direction. We show that use of uniform grids combined, where possible, with the Richardson extrapolation can significantly improve results. We show also that the mesh stretching can significantly speed up the convergence, but there can be also a certain loss of accuracy.

2. FORMULATION OF THE PROBLEMS AND NUMERICAL METHOD

We study stability of steady convective flows of a Boussinesq fluid with kinematic viscosity ν^* and thermal diffusivity χ^* in a cavity of length L^* and height H^*. The vertical boundaries of the cavity have constant temperatures θ^*_{hot} and θ^*_{cold}, while the horizontal ones are perfectly thermally insulated or are perfectly conducting. The vertical and lower boundaries are no-slip. The upper boundary can be no-slip or stress-free or account for the effect of thermocapillarity. The flow is described by the momentum, continuity and energy equations in a Cartesian coordinate system (x^*, y^*). To render the equations dimensionless we use the scales $D^* = \text{Min}(H^*, L^*)$, D^{*2}/ν^*, ν^*/D^*, $\rho^*(\nu^*/D^*)^2$ for length, time, velocity and pressure, respectively. The temperature is rendered dimensionless by the relation $\theta = (\theta^* - \theta^*_{\text{cold}})/(\theta^*_{\text{hot}} - \theta^*_{\text{cold}})$. The set of Boussinesq equations for the non-dimensional velocity $\mathbf{v} = \{v_x, v_y\}$, temperature θ and pressure p in the rectangular domain $0 \leqslant x \leqslant A_x$, $0 \leqslant y \leqslant A_y$, reads

$$\frac{\partial \mathbf{v}}{\partial t} + (\mathbf{v} \cdot \nabla)\mathbf{v} = -\nabla p + \Delta \mathbf{v} + Gr\,\theta\,\mathbf{e}_y \tag{1}$$

$$\frac{\partial \theta}{\partial t} + (\mathbf{v} \cdot \nabla)\theta = \frac{1}{Pr}\,\Delta\theta \tag{2}$$

$$\nabla \cdot \mathbf{v} = 0 \tag{3}$$

Here $A_x = L^*/D^*$, $A_y = H^*/D^*$ are the aspect ratios of the cavity (apparently, one of them is exactly one), $Gr = g^*\beta^*(\theta^*_{\text{hot}} - \theta^*_{\text{cold}})D^{*3}/\nu^{*2}$ the Grashof number, $Pr = \nu^*/\chi^*$ the Prandtl number, g^* gravity acceleration, β^* the thermal expansion coefficient, and $\mathbf{e}_y$ the unit vector in the y-direction.

The vertical and lower boundaries are no-slip

$$v_x = v_y = 0 \quad \text{at } x = 0 \text{ and } A_x, \text{ and } y = 0 \tag{4}$$

The upper boundary can be either no-slip

$$v_x = v_y = 0 \quad \text{at } y = A_y \tag{5a}$$

or to be a 'free' surface with the thermocapillary force acting along it

$$v_y = 0, \quad \frac{\partial v_x}{\partial y} = -MaPr\frac{\partial \theta}{\partial x} \quad \text{at } y = A_y \tag{5b}$$

Here $Ma = -\gamma^*(\theta^*_{\text{hot}} - \theta^*_{\text{cold}})D^*/\rho^*\nu^*\chi^*$ is the Marangoni number, where ρ^* is the density and $\gamma^* = \partial\alpha^*/\partial\theta^*$ describes the dependence of the surface tension α^* on the temperature, assuming that the dependence is linear. Apparently, $Ma = 0$ corresponds to the stress-free boundary.

DOI: 10.1002/fld

Constant temperatures are prescribed at the vertical boundaries

$$\theta = 1 \text{ at } x = 0 \quad \text{and} \quad \theta = 0 \text{ at } x = A_x \tag{6}$$

while the horizontal boundaries can be perfectly insulated

$$\partial\theta/\partial y = 0 \quad \text{at } y = 0 \text{ and } A_y \tag{7a}$$

or perfectly conducting

$$\theta = 1 - x/A_x \quad \text{at } y = 0 \text{ and } A_y \tag{7b}$$

Problems (1)–(7) is solved by a standard finite volume method as described in Reference [30]. Non-linear terms are approximated by the conservative central differencing scheme, for which we have several reasons. First, stability studies usually require conservative schemes, so that no artificial viscosity appears. Second, with the mesh refinement the grid Reynolds and Peclet numbers decrease, so that the conservative scheme satisfies the three conditions of Patankar [30]. Third, the issues of numerical stability of a straightforward time integration are not relevant for this study because steady state are calculated by the Newton iteration (see below).

The finite volume grid is staggered and can be uniform or stretched. The effect of stretching is also discussed below. The scalar variables θ and p, as well as divergence of velocity, are calculated at the nodes with integer indices $[x_i, y_j]$. The components of velocity $u = v_x$ and $w = v_y$ are calculated in the points $[x_{i+1/2}, y_j]$ and $[x_i, y_{j+1/2}]$, respectively, where $x_{i+1/2} = (x_i + x_{i+1})/2$ and $y_{j+1/2} = (y_j + y_{j+1})/2$. Denoting by square brackets with subscripts $[\bullet]_{i,j}$ approximation of a term in the appropriate grid node, the resulting system of steady equations reads

$$\left[u\frac{\partial u}{\partial x}\right]_{i+1/2,j} + \left[w\frac{\partial u}{\partial y}\right]_{i+1/2,j} = -\left[\frac{\partial p}{\partial x}\right]_{i+1/2,j} + \left[\frac{\partial^2 u}{\partial x^2} + \frac{\partial^2 u}{\partial y^2}\right]_{i+1/2,j} \tag{8a}$$

$$\left[u\frac{\partial w}{\partial x}\right]_{i,j+1/2} + \left[w\frac{\partial w}{\partial y}\right]_{i,j+1/2} = -\left[\frac{\partial p}{\partial y}\right]_{i,j+1/2} + \left[\frac{\partial^2 w}{\partial x^2} + \frac{\partial^2 w}{\partial y^2}\right]_{i,j+1/2} + \frac{Gr}{2}(\theta_{ij} + \theta_{i,j+1}) \tag{8b}$$

$$\left[\frac{\partial u}{\partial x}\right]_{i,j} + \left[\frac{\partial w}{\partial y}\right]_{i,j} = 0 \tag{8c}$$

$$\left[u\frac{\partial \theta}{\partial x}\right]_{i,j} + \left[w\frac{\partial \theta}{\partial y}\right]_{i,j} = \frac{1}{Pr}\left[\frac{\partial^2 \theta}{\partial x^2} + \frac{\partial^2 \theta}{\partial y^2}\right]_{i,j} \tag{8d}$$

The indices i and j vary from 1 to N_x and N_y, respectively. Equations (8) are used for calculation of steady-state flows. Assuming that $\{\tilde{u}(x, y), \tilde{w}(x, y), \tilde{\theta}(x, y), \tilde{p}(x, y)\}e^{\lambda t}$ is an infinitesimally small perturbation, the linear stability eigenproblem written for a calculated steady-state

DOI: 10.1002/fld

U, W, T, P reads

$$\lambda\tilde{u}_{i+1/2,j} = -\left[U\frac{\partial\tilde{u}}{\partial x}\right]_{i+1/2,j} - \left[\tilde{u}\frac{\partial U}{\partial x}\right]_{i+1/2,j} - \left[W\frac{\partial\tilde{u}}{\partial y}\right]_{i+1/2,j} - \left[\tilde{w}\frac{\partial U}{\partial y}\right]_{i+1/2,j} - \left[\frac{\partial\tilde{p}}{\partial x}\right]_{i+1/2,j} + \left[\frac{\partial^2\tilde{u}}{\partial x^2} + \frac{\partial^2\tilde{u}}{\partial y^2}\right]_{i+1/2,j} \tag{9a}$$

$$\lambda\tilde{w}_{i,j+1/2} = -\left[U\frac{\partial\tilde{w}}{\partial x}\right]_{i,j+1/2} - \left[\tilde{u}\frac{\partial W}{\partial x}\right]_{i,j+1/2} - \left[W\frac{\partial\tilde{w}}{\partial y}\right]_{i,j+1/2} - \left[\tilde{w}\frac{\partial W}{\partial y}\right]_{i,j+1/2} - \left[\frac{\partial\tilde{p}}{\partial y}\right]_{i,j+1/2} + \left[\frac{\partial^2\tilde{w}}{\partial x^2} + \frac{\partial^2\tilde{w}}{\partial y^2}\right]_{i,j+1/2} + \frac{Gr}{2}(\tilde{\theta}_{ij} + \tilde{\theta}_{i,j+1}) \tag{9b}$$

$$0 = \left[\frac{\partial\tilde{u}}{\partial x}\right]_{i,j} + \left[\frac{\partial\tilde{w}}{\partial y}\right]_{i,j} \tag{9c}$$

$$\lambda\tilde{\theta}_{i,j} = -\left[U\frac{\partial\tilde{\theta}}{\partial x}\right]_{i,j} - \left[u\frac{\partial T}{\partial x}\right]_{i,j} - \left[W\frac{\partial\tilde{\theta}}{\partial y}\right]_{i,j} - \left[w\frac{\partial T}{\partial y}\right]_{i,j} + \frac{1}{Pr}\left[\frac{\partial^2\tilde{\theta}}{\partial x^2} + \frac{\partial^2\tilde{\theta}}{\partial y^2}\right]_{i,j} \tag{9d}$$

These equations can be written in the matrix form as

$$\lambda\mathbf{B}\begin{pmatrix}\tilde{u}\\ \tilde{w}\\ \tilde{p}\\ \tilde{\theta}\end{pmatrix} = \mathbf{J}\begin{pmatrix}\tilde{u}\\ \tilde{w}\\ \tilde{p}\\ \tilde{\theta}\end{pmatrix} \tag{10}$$

where $\mathbf{J}$ is the Jacobian matrix calculated from the r.h.s. of (9) and $\mathbf{B}$ is the diagonal matrix such that its diagonal elements corresponding to the values of $\tilde{u}, \tilde{w}, \tilde{\theta}$ are equal to one, while the elements corresponding to $\tilde{p}$ are zeros. This necessarily yields $\det\mathbf{B} = 0$, so that the generalized eigenproblem (10) cannot be transformed into a standard eigenproblem. Apparently, $\mathrm{Real}(\lambda) > 0$ means instability of the steady flow state.

Considering the linear stability of steady-state flows, we are looking for the values of the Grashof or Marangoni numbers, for which the real part of at least one eigenvalue λ changes its sign from negative to positive. This eigenvalue is called 'leading' and the corresponding values of the governing parameters are called critical and are denoted as Gr_{cr} and Ma_{cr}. The imaginary part $\omega_{\mathrm{cr}} = \mathrm{Im}(\lambda)$ of the leading eigenvalue corresponding to $\mathrm{Real}(\lambda) = 0$ yields the frequency of the most unstable perturbation at the critical point and is called 'critical frequency'. The spatial pattern of the most unstable perturbation is yielded by the eigenvector of (10). Since the eigenvector is complex and is defined to within a multiplication by a complex constant, we usually plot its absolute value, whose pattern is constant independent.

DOI: 10.1002/fld

The eigenproblem (10) is solved by the Arnoldi iteration in the shift-and-invert mode

$$(\mathbf{J}-\sigma\mathbf{B})^{-1}\mathbf{B}\begin{pmatrix}\tilde{u}\\ \tilde{w}\\ \tilde{p}\\ \tilde{\theta}\end{pmatrix}=\mu\begin{pmatrix}\tilde{u}\\ \tilde{w}\\ \tilde{p}\\ \tilde{\theta}\end{pmatrix},\quad \mu=\frac{1}{\lambda-\sigma} \tag{11}$$

where σ is a complex shift. The ARPACK package [29][‡] is used. This approach succeeds when the shift σ is chosen close to the leading eigenvalue λ. It is an easy task for benchmark problems considered here, where the estimate of λ is known. However, it is an additional difficulty for each new problem where no information on the stability properties of the flow is available.

The computational process proceeds as follows. At the first stage we apply Jacobian-full exact Newton iteration to calculate a steady flow state. Then the linear stability of the calculated steady flow is studied by applying the shift-and-invert Arnoldi iteration to the corresponding eigenvalue problem with the secant method used for the calculation of a critical parameter value. The key issue for the effectiveness of both Newton and Arnoldi iteration techniques is a fast solution of the systems of linear algebraic equation, which is needed at every Newton iteration, as well as for building the Krylov basis for the Arnoldi iteration. The traditional approach here is application of modern Krylov-subspace-based iteration methods like preconditioned GMRES and BiCGstab [24–27]. Studies [24–26] reported several hours of computations on massively parallel computers needed to calculate a critical value. Here we describe another approach, which is based on the fact that the matrix $(\mathbf{J}-\sigma\mathbf{B})^{-1}$ remains unchanged during the whole Arnoldi iteration process. Thus, if it was computed the calculation of a next vector of the Krylov basis is reduced to a single matrix–vector multiplication, which is expected to be much faster than any iterative solver. The calculation of the inverse matrix $(\mathbf{J}-\sigma\mathbf{B})^{-1}$ is possible, but requires too many arithmetic operations and too much memory to store the result. Instead of that one can calculate the **LU**-decomposition of the matrix $(\mathbf{J}-\sigma\mathbf{B})$, which is much faster, and due to the high level of sparseness of $(\mathbf{J}-\sigma\mathbf{B})$ does not require too much memory to be stored. Then the next vector of the Krylov basis is calculated by two back substitutions, which consumes the CPU time comparable with the matrix–vector multiplication. Apparently, the two back substitutions always require the same CPU time to be completed, and are expected to be much faster than any iterative solver. Then, the efficiency of the whole approach is defined by a possibility of an efficient computations of the **LU**-decomposition. This can be achieved by use of modern multifrontal direct solvers for sparse matrices (we use the MUMPS solver[§]). The characteristic times and comparison with Reference [25] are reported in Appendix A.

A more unexpected observation was that the multifrontal direct solver was rather efficient also for the Newton iteration. In this case the **LU**-decomposition must be performed at every iteration, and therefore can be expected to be slower than a modern preconditioned iterative technique. On the other hand, in the computations described below the calculation of a steady-state was significantly faster than the forthcoming eigenvalue computation (see Appendix A), so that further improvement

[‡]See http://www.caam.rice.edu/software/ARPACK/

[§]See http://www.enseeiht.fr/apo/MUMPS/ or http://grall.ens-lyon.fr/MUMPS/

DOI: 10.1002/fld

of the Newton iteration linear solver was not very significant. The explanation for that may be connected with a very large level of sparseness of the matrices produced by the second-order finite volume method we use. It is clear that the effectiveness of a sparse matrix direct solver reduces rapidly with the decrease of the sparseness. Therefore the observed efficiency of the direct solver described here may disappear when higher-order methods leading to denser matrices are applied.

It is difficult to present exact CPU-times, since they are always problem dependent, i.e. different problems need different number of Newton and Arnoldi iterations. We can stay that calculation of critical Grashof number, which includes four to six solutions for steady-state flows followed by solution of the eigenvalue problem, using the grid 450×450 consumes less than 2 CPU hours on Itanium-2 personal workstation. In fact, further grid refinement is restricted by available computer memory, which is needed for the direct solver producing the **LU** decompositions. More details on the consumed memory and CPU time, regarding one of the problems considered below, are given in Appendix A.

3. RESULTS

List of the benchmark problems considered and comparison with the independent data are shown in Table I. We usually compare with results of the global Galerkin method [12], for which the convergence to within several decimal digits can be established. The details and comparison with the results of other authors can be found in References [9–13].

3.1. Buoyancy convection benchmarks

First we consider several benchmark problems dealing with buoyancy convection in rectangular cavities. These are problems 1–7 with the boundary conditions and parameters shown in Table I. Problems 4–7 are well-known benchmarks formulated in References [3, 6, 8]. We add also problems of convection of a low-Prandtl-number fluid in a square cavity (problems 1 and 2) and the problem of convection of air in a square cavity with perfectly conducting horizontal walls (problem 3).

To illustrate the convergence and the importance of the Richardson extrapolation we show the results obtained for problem 2 in Table II. The results are reported for the uniform grids with number of nodes gradually increased by an increment 10. The results are compared with the result of Reference [10] (the last row of Table II) obtained by the global Galerkin method and converged at least to within the fourth decimal digit. It is seen that with the use of 200^2 nodes we obtain three correct digits in the critical Grashof number and two correct digits in the critical frequency. However, even with the grid of 450^2 nodes we still do not obtain the correct fourth digit of the critical parameters. At the same time, applying the Richardson extrapolation for two consequent grids we observe a very good agreement with the results of Reference [10] already starting from the grid with 100^2 nodes. The Richardson extrapolation using 190^2 and 200^2 grids already yields four correct decimal digits in both critical Grashof number and critical frequency.

Figure 1 shows the convergence of the critical parameters for problems 1–4 comparing to the result of the Richardson extrapolation based on 440^2 and 450^2 nodes. The fastest convergence is observed for the problem 3, which was observed also for the convergence of the global Galerkin method reported in Reference [13]. The replacement of the perfectly conducting horizontal walls of the problem 3 by the perfectly insulated ones of the problem 4 leads to a development of very thin thermal boundary layers along the vertical boundaries, which drastically slows down the

DOI: 10.1002/fld

Table I. Benchmark problems solved, finest results and comparison with the independent data.

Problem	A_x	A_y	Pr	Ma	Finest grid	b.c. on horizontal boundaries	Converged Gr_{cr}/ω_{cr}	Independent result Gr_{cr}/ω_{cr}	Source
1	1	1	0	—	450×450	(5.1) + (7.1)	$9.471\times10^5/8249$	$9.472\times10^5/8242$	[1]
2	1	1	0.015	—	450×450	(5.1) + (7.1)	$2.908\times10^6/8597$	$2.908\times10^6/8597$	[1]
3	1	1	0.71	—	450×450	(5.1) + (7.2)	$2.969\times10^6/2745$	$2.969\times10^6/2745$	[12]
4	1	1	0.71	—	450×450	(5.1) + (7.1)	$2.566\times10^8/5570$	$2.567\times10^8/5559$	[12]
5	4	1	0.015	—	600×150	(5.1) + (7.1)	$1.3199\times10^5/123.455$	$1.3198\times10^5/123.452$	[1]
6	4	1	0.015	—	600×150	(5.2) + (7.1)	77 451/1497.99	77 452/1498.01	[1]
7	1	8	0.71	0	150×1200	(5.2) + (7.1)	$4.3097\times10^5/1121.98$	$4.3126\times10^5/1122.35$	[11]
Problem	A_x	A_y	Pr	Gr	Finest grid	b.c. on horizontal boundaries	Converged Ma_{cr}/ω_{cr}	Independent result Ma_{cr}/ω_{cr}	Source
8	2.5	1	6.78	0	400×200	(5.2) + (7.1)	24 679/89.22	24 239/(not reported)	[31]
9	4	1	0.015	0	800×200	(5.2) + (7.1)	4779/6674	4781/6674	—

DOI: 10.1002/fld

Table II. Convergence of critical Grashof number and critical frequency for the problem 2.

$N = N_x \times N_y$	Gr_{cr}	$\omega_{\mathrm{cr}}/\sqrt{Gr_{\mathrm{cr}}}$	ω_{cr}
50	3 014 437	4.78819	8313.32
60	2 984 090	4.86574	8405.33
70	2 961 670	4.91382	8456.44
80	2 947 121	4.96442	8522.51
90	2 937 725	4.96584	8511.35
100	2 931 324	4.98066	8527.44
Richardson, 90–100	**2 904 036**	**5.04384**	**8596.06**
110	2 926 929	4.99143	8539.47
120	2 923 709	4.99954	8548.64
130	2 921 275	5.00582	8555.82
140	2 919 384	5.01076	8561.49
150	2 917 886	5.01473	8566.07
160	2 916 678	5.01797	8569.83
170	2 915 687	5.02064	8572.94
180	2 914 865	5.02288	8575.55
190	2 914 174	5.02477	8577.76
200	2 913 589	5.02639	8579.66
Richardson, 190–200	**2 908 174**	**5.04139**	**8597.29**
210	2 913 087	5.02777	8581.28
220	2 912 655	5.02896	8582.68
230	2 912 280	5.03001	8583.92
240	2 911 951	5.03093	8585.01
250	2 911 662	5.03173	8585.94
260	2 911 406	5.03245	8586.79
270	2 911 179	5.03309	8587.55
280	2 910 976	5.03366	8588.22
290	2 910 794	5.03417	8588.82
300	2 910 615	5.03465	8589.38
Richardson, 290–300	**2 908 063**	**5.04149**	**8597.29**
310	2 910 447	5.03507	8589.85
320	2 910 345	5.03545	8590.34
330	2 910 223	5.03580	8590.76
340	2 910 110	5.03611	8591.12
350	2 910 011	5.03640	8591.47
360	2 909 917	5.03666	8591.78
370	2 909 832	5.03691	8592.08
380	2 909 753	5.03713	8592.34
390	2 909 679	5.03734	8592.58
400	2 909 613	5.03753	8592.81
Richardson, 390–400	**2 908 341**	**5.04121**	**8597.21**
410	2 909 558	5.03770	8593.00
420	2 909 499	5.03786	8593.20
430	2 909 445	5.03801	8593.38
440	2 909 396	5.03815	8593.56
450	2 909 349	5.03829	8593.72
Richardson, 440–450	**2 908 327**	**5.04121**	**8597.19**
Result of Reference [10]	2 908 332	5.04121	8597.19

DOI: 10.1002/fld

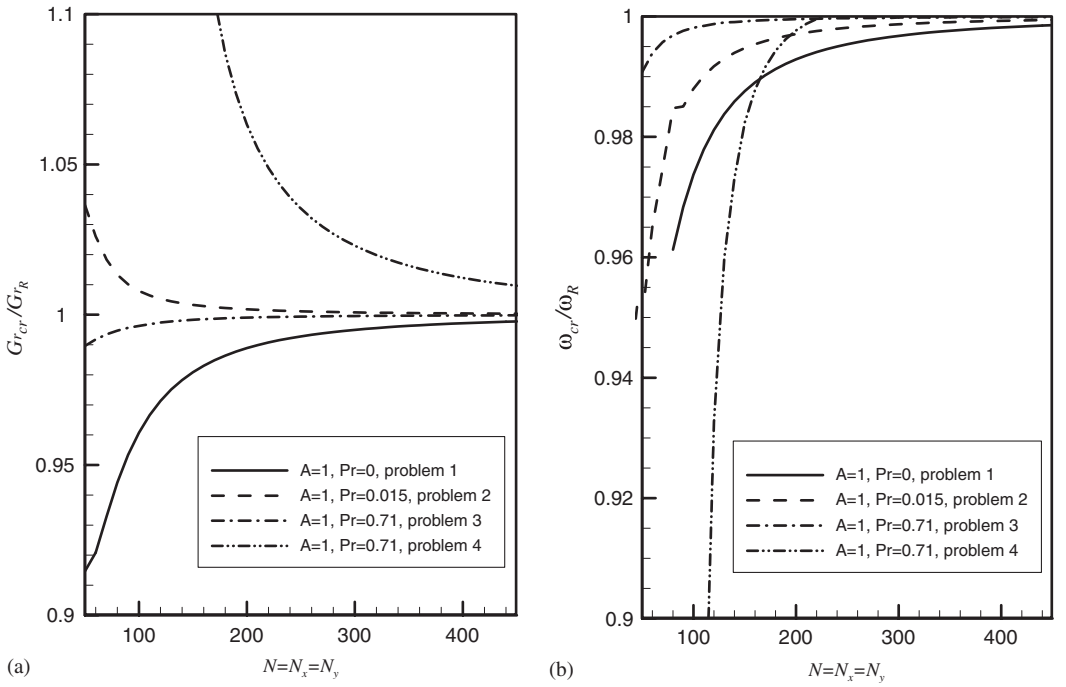

Figure 1. Convergence of the critical Grashof number and critical frequency for convection in a square cavity with different Prandtl numbers and boundary conditions. The subscript R stays for the Richardson extrapolation from the two finest grids.

convergence. This is also similar to the observations of Reference [13] made for the convergence of the global Galerkin method. For the flows with a small Prandtl number, i.e. problems 1 and 2, we observe that the convergence for $Pr=0$ is significantly slower than that for $Pr=0.015$, in spite of the lower value of the critical Grashof number for $Pr=0$ (Table I). The explanation of that also is connected with the boundary layers, which develop near the no-slip walls in the case $Pr=0$. With the increase of the Prandtl number the temperature gradient near the walls decreases and these boundary layers smear out, which yields a smoother spatial pattern of the most unstable perturbation. Consequently, a faster convergence of the stability parameters is observed. The corresponding perturbation patterns are reported in Reference [12].

For the calculations in elongated cavities with $A_x \neq A_y$ we usually use grids with $N_x = (A_x/A_y)N_y$ to keep the finite volume square or at least close to the square shape. Figure 2 shows the convergence of the critical parameters for the benchmark problem of Reference [6]. For horizontally elongated cavities with $A_x=4$ and $A_y=1$ the convergence of the critical Grashof number is similar for a no-slip or stress-free upper surface (Figure 2(a)). At the same time the convergence of the critical frequency is slightly slower for the stress-free upper boundary (Figure 2(b)). Note, that to obtain the convergence to within 1% error one needs calculations using $N_x>350$ (see Figure 2(a)). As above, the use of Richardson extrapolation can significantly improve the result already starting with $N_x=200$. Thus, the values of critical Grashof number for problem 5 calculated on the grids 200×50 and 240×60 are 1.361×10^5 and 1.348×10^5, respectively.

DOI: 10.1002/fld

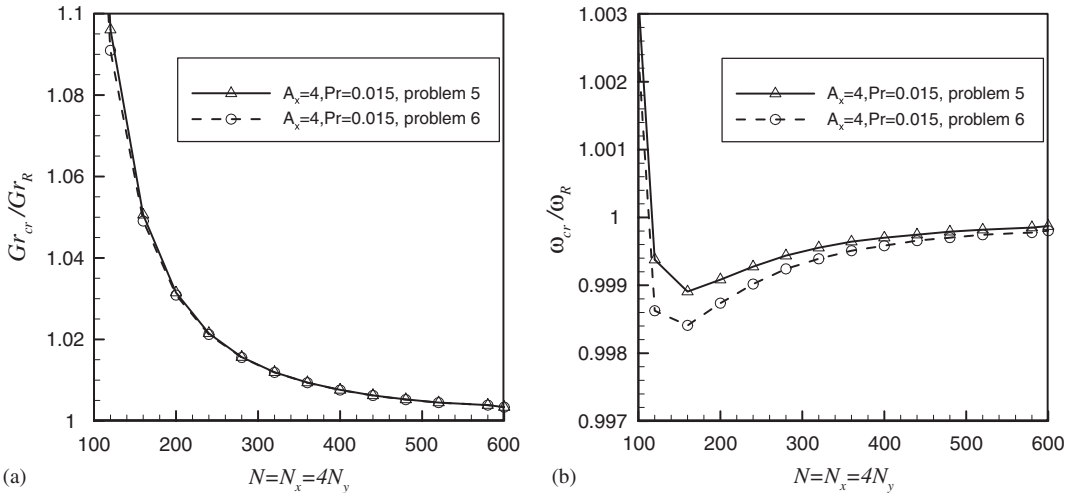

Figure 2. Convergence of the critical Grashof number and critical frequency for convection in a cavity $A_x = 4$, $A_y = 1$ for different boundary conditions. $Pr = 0.015$. The subscript R stays for the Richardson extrapolation from the two finest grids.

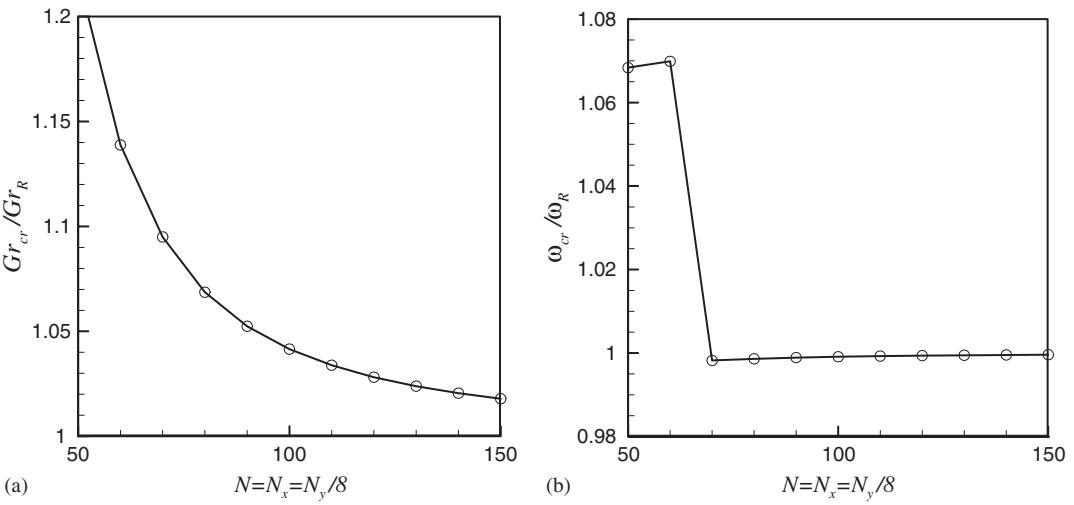

Figure 3. Convergence of the critical Grashof number and critical frequency for convection of air ($Pr = 0.71$) in a cavity $A_x = 1$, $A_y = 8$. The subscript R stays for the Richardson extrapolation from the two finest grids.

The converged value is 1.3198×10^5. The Richardson extrapolation based on the two grids yields the value 1.3183×10^5, which is significantly closer to the converged one.

Another example considers a recent benchmark problem on oscillatory instability of convection of air in a tall vertical cavity with $A_x = 1$ and $A_y = 8$ [8]. Solution of this benchmark problem by the global Galerkin method is reported in Reference [11]. Here, in Figure 3, we illustrate

DOI: 10.1002/fld

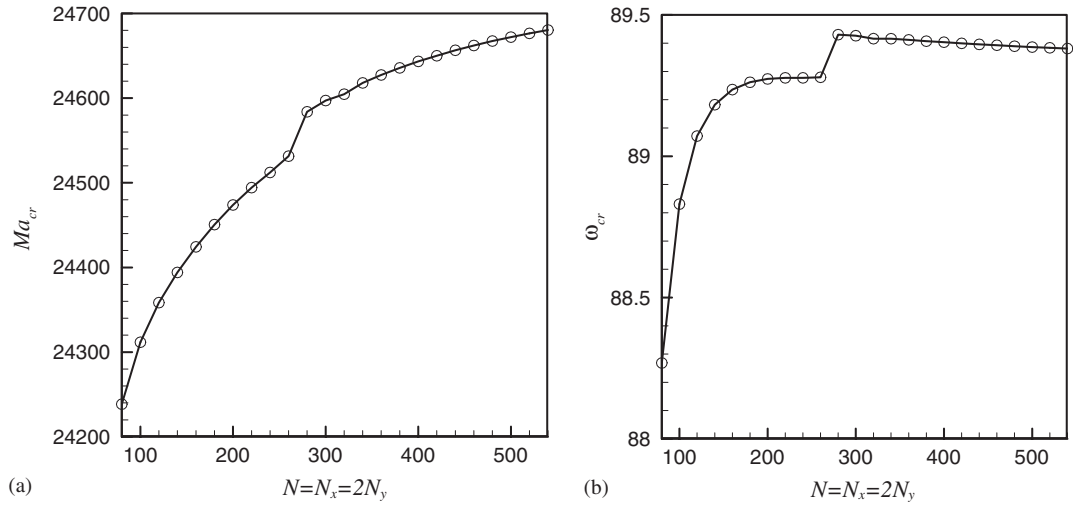

Figure 4. Convergence of the critical Marangoni number and critical frequency for thermocapillary convection of water ($Pr=6.78$) in a cavity $A_x=2.5$, $A_y=1$.

convergence of the critical parameters for the finite volume method. In this case convergence of the critical frequency is much faster than that of the critical Grashof number. The value of Gr_{cr} is still within approximately 2% error on the finest grid used consisted of 150×1200 nodes. Again, the Richardson extrapolation based on the grids 140×1120 and 150×1200 yields the value $Gr_{\mathrm{cr}}=4.3097\times10^5$, which is very close to the converged value 4.3126×10^5 calculated in Reference [11].

3.2. *Thermocapillary convection flows*

The benchmark-quality data on Marangoni–Bénard instability was reported in Reference [32] for heating from below. It is rather surprising that a commonly accepted benchmark problem for the thermocapillary convection in a rectangular cavity heated from the side was not formulated. Here, for the benchmark purposes, we consider the two following problems. The first problem is taken from the study [31] and deals with the thermocapillary convection of fluid with $Pr=6.78$, characteristic for water, in a rectangular cavity with $A_x=2.5$ and $A_y=1$. The second problem is based on geometry of the benchmark problem [6] and considers the thermocapillary convection of a low-Prandtl-number ($Pr=0.015$) fluid in a cavity with $A_x=4$ and $A_y=1$.

In the case of the thermocapillary convection the x-velocity boundary conditions (4) and (5b) are discontinuous at the corner points $x=0$ and A_x and $y=A_y$. This means that the convergence of the grid step Taylor series cannot be expected at least in the vicinity of the corner points, so that the Richardson extrapolation cannot be applied here. The independent results on the thermocapillary convection with which we can compare are also not very precise. Therefore, we report the convergence of the critical numbers themselves without comparing them to any independent result or their Richardson extrapolation. Together with the convergence results we report the flow patterns and the patterns of the most unstable perturbations. The latter, to the best of our knowledge, were never reported before.

DOI: 10.1002/fld

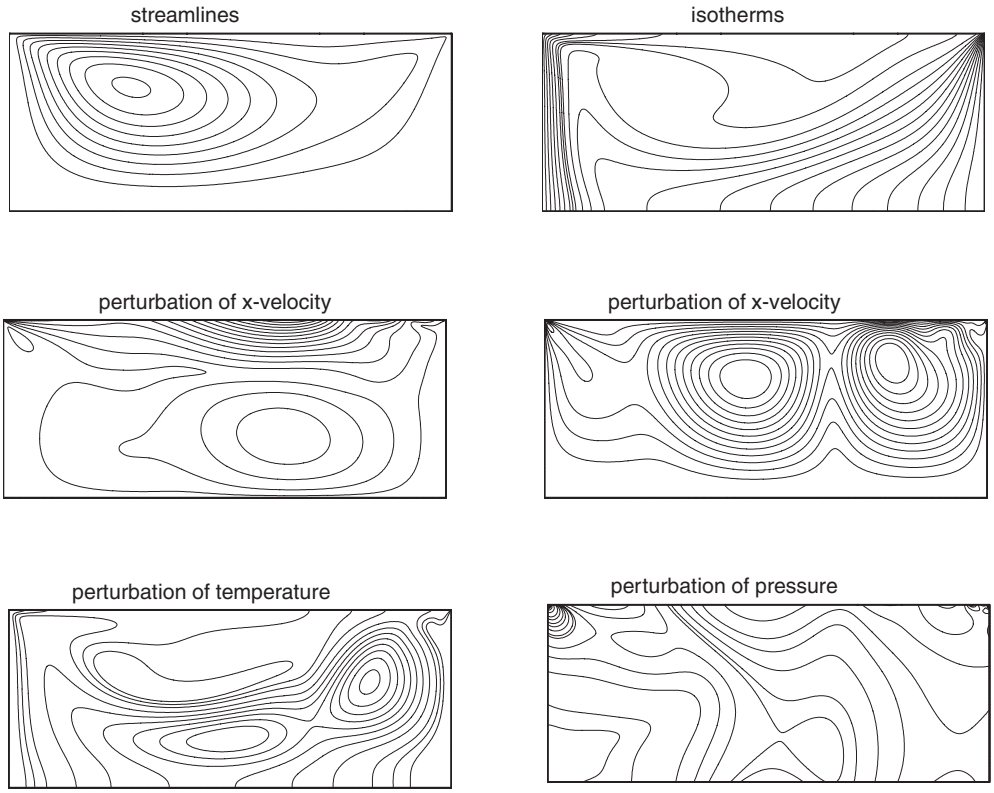

Figure 5. Patterns of flow and most unstable perturbation at the critical Marangoni number for thermocapillary convection of water ($Pr = 6.78$) in a cavity $A_x = 2.5$, $A_y = 1$.

The convergence of the critical parameters for the problem 8 is shown in Figure 4. It is seen that the convergence is not yet completely established even for $N_x = 2N_y = 540$. Further grid refinement was not possible because of computer memory restrictions. The finest result of $Ma_{cr}/Pr = 3640$ is rather well compared with the result of Reference [31], which is 3575. At the same time the comparison can be only qualitative since the critical frequency, as well as the perturbation patterns, was not reported in Reference [31]. It is also seen (Figure 4) that there is a steep change in the critical numbers for the number of grid points changing between $N_x = 2N_y = 300$ and 400. This is explained by the qualitatively accurate resolution of the perturbation pattern, which is observed only starting from $N_x = 2N_y \approx 360$.

The flow patterns and the patterns of the most unstable perturbations for the problem 8 are shown in Figure 5. It is seen that due to a relatively large Prandtl number the thermal boundary layer is developed near the cold (left) vertical wall. There is also a steep temperature change observed in the upper right corner of the cavity. These lead to large local temperature gradients, which causes steep changes in the thermocapillary force. The latter can be the main reason for the slow convergence observed.

DOI: 10.1002/fld

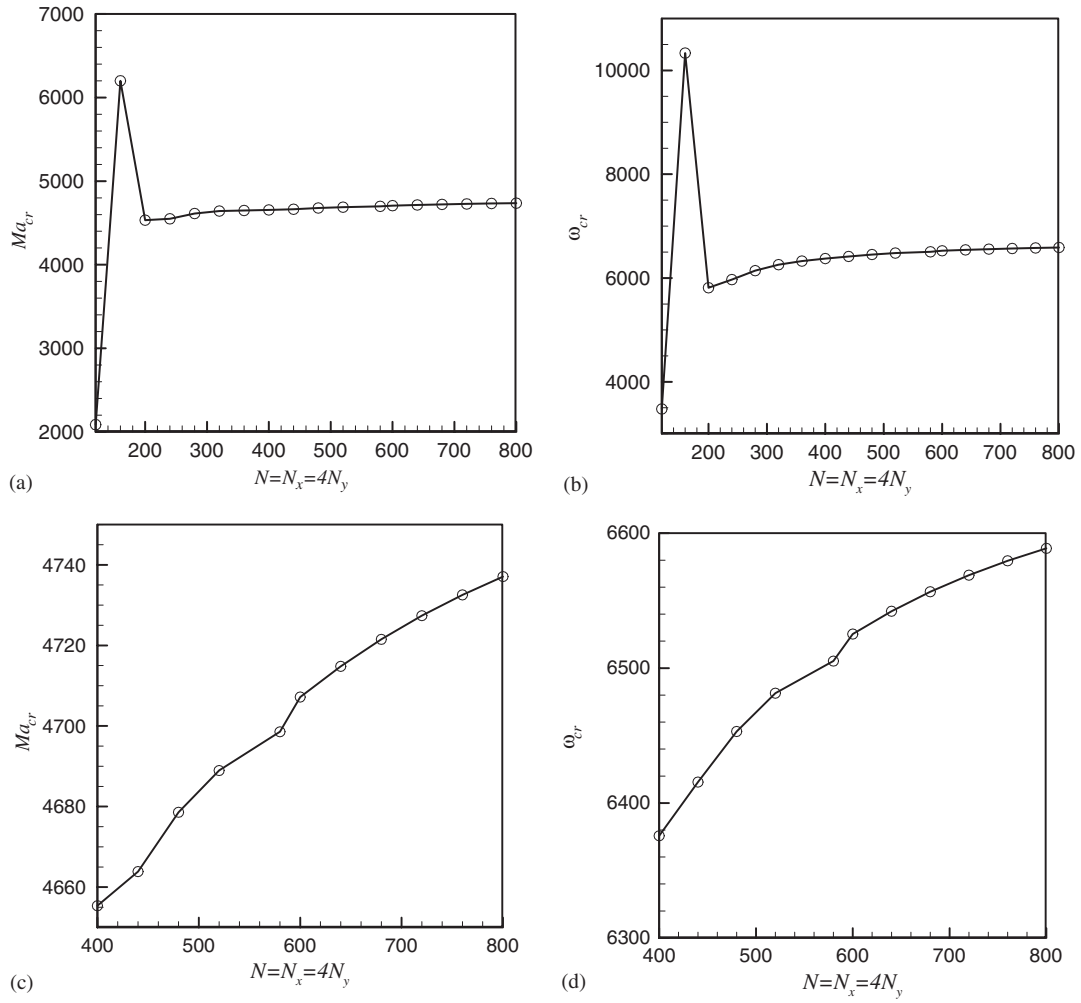

Figure 6. Convergence of the critical Marangoni number and critical frequency for thermocapillary convection of low-Prandtl-number fluid ($Pr = 0.015$) in a cavity $A_x = 4$, $A_y = 1$.

The convergence for the problem 9 is illustrated in Figure 6. Beyond $N_x = 4N_y = 300$ grid points the change of the critical parameters becomes slow (Figures 6(a) and (b)). However, as it follows from the zoomed Figures 6(c) and (d) the convergence is not completely reached even at $N_x = 4N_y = 800$. To validate the results we tried to carry out the stability calculations using the global Galerkin method used in References [1–13]. However, with this method also we were not able to establish a complete convergence. The best values obtained by both methods are compared in Table I, which shows a good agreement. A good agreement is observed also in the patterns of the most unstable perturbations obtained by the two methods. The perturbations are shown in Figure 7. Steep maxima of the perturbation amplitudes observed is the main reason for the slow convergence of the critical parameters. Since the instability in this problem sets in inside the bulk

DOI: 10.1002/fld

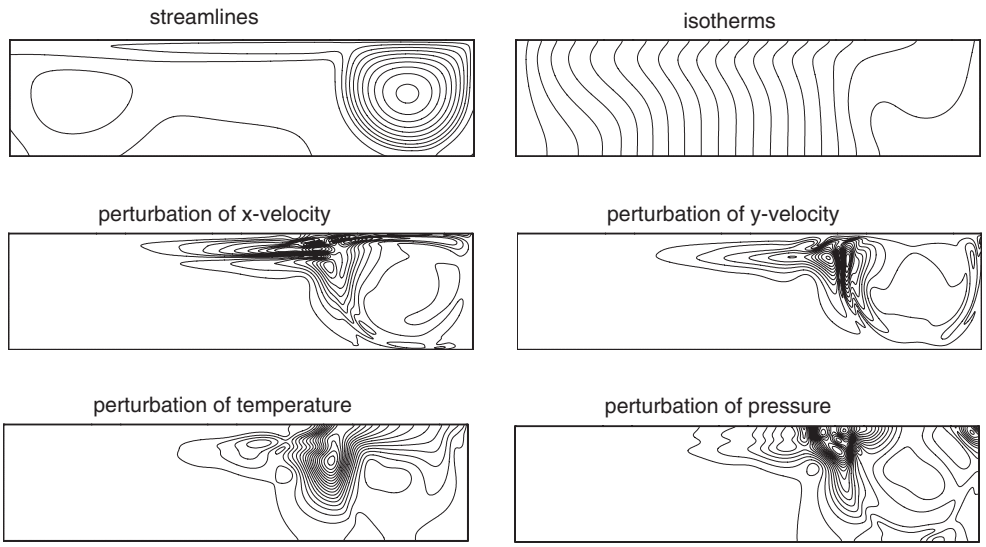

Figure 7. Patterns of flow and most unstable perturbation at the critical Marangoni number for thermocapillary convection of low-Prandtl-number fluid ($Pr = 0.015$) in a cavity $A_x = 4$, $A_y = 1$.

of the flow and not in a boundary layer its calculation requires a good global resolution. A usual mesh stretching near the boundaries will not be helpful here. Because of these difficulties it is the author's opinion that this case can be a good modern benchmark problem.

3.3. Effect of the stretching

Since there is an infinite amount of stretching possibilities it is impossible to obtain a full answer on the question which stretching is optimal for a certain problem. Here we study the following stretching. The uniform grid defined in the nodes x_i and y_j is transformed into a stretched one by

$$x_i \leftarrow A_x \left[\frac{x_i}{A_x} - a \sin\left(2\pi \frac{x_i}{A_x}\right) \right], \quad y_j \leftarrow A_y \left[\frac{y_j}{A_y} - b \sin\left(2\pi \frac{y_j}{A_y}\right) \right] \tag{12}$$

After the transformation defined by (12) the grid becomes stretched near the boundaries. The density of the stretching is defined by the parameters a and b which vary between 0 and 0.12.

The process of the adaptation of the parameters a and b to a certain problem is illustrated in Tables III and IV. For problems 1 and 4 of convection in a square cavity we performed calculations using $N_x = N_y = 200$ and varying a and b. We are looking for a combination of these two parameters yielding the critical Grashof number, which is most close to the Richardson extrapolation based on the uniform meshes with $N_x = N_y = 440$ and 450. Thus, the optimal parameters for the problem 1 are found to be $a = b = 0.08$ and $a = 0.05$ and $b = 0.03$ for the problem 4. These parameters are shown in bold in Tables III and IV.

DOI: 10.1002/fld

Table III. Results for different stretching parameters for problem 1. $N = N_x \times N_y = 200$.

a	b	Gr_{cr}	$\omega_{\mathrm{cr}}/\sqrt{Gr_{\mathrm{cr}}}$
0	0	936 608	8.4161
0.01	0	937 043	8.4188
0.05	0	938 276	8.4269
0.07	0	638 536	8.4291
0.08	0	938 569	8.4296
0.09	0	938 536	8.4298
0.1	0	938 444	8.4297
0.11	0	938 289	8.4292
0.08	0.05	940 241	8.4405
0.08	0.07	940 495	8.4426
0.08	**0.08**	**940 525**	**8.4432**
0.08	0.09	940 491	8.4434
0.09	0.08	940 489	8.4434
0.07	0.08	940 494	8.4426
Richardson extrapolation from uniform grid		*947 166*	*8.476715*

Table IV. Results for different stretching parameters for problem 4. $N = N_x \times N_y = 200$.

a	b	Gr_{cr}	$\omega_{\mathrm{cr}}/\sqrt{Gr_{\mathrm{cr}}}$
0	0	0.27287	0.34615
0.01	0	0.26863	0.34672
0.02	0	0.26481	0.34709
0.03	0	0.26132	0.34729
0.04	0	0.25808	0.34731
0.05	0	0.25502	0.34718
0.06	0	0.25210	0.34689
0.05	0.01	0.25552	0.34675
0.05	0.02	0.25604	0.34636
0.05	**0.03**	**0.25656**	**0.34602**
0.05	0.04	0.25710	0.34572
Richardson's extrapolation from uniform grid		*0.2566354*	*0.3477536*

Figures 8 and 9 illustrate the convergence of the critical parameters calculated for the optimal values of a and b found. These results are compared with the results obtained using the uniform grid and the grid with a very dense stretching defined by $a = b = 0.12$.

For the problem 1 (Figure 8) there is almost no difference between the stretching with $a = b = 0.08$ or 0.12. The convergence is slightly faster for the optimized values of a and b equal to 0.08. In the case of uniform grid the convergence is slower, especially for the critical frequency. At the same time, at large values of N_x and N_y we observe that there is almost no difference between different grids.

DOI: 10.1002/fld

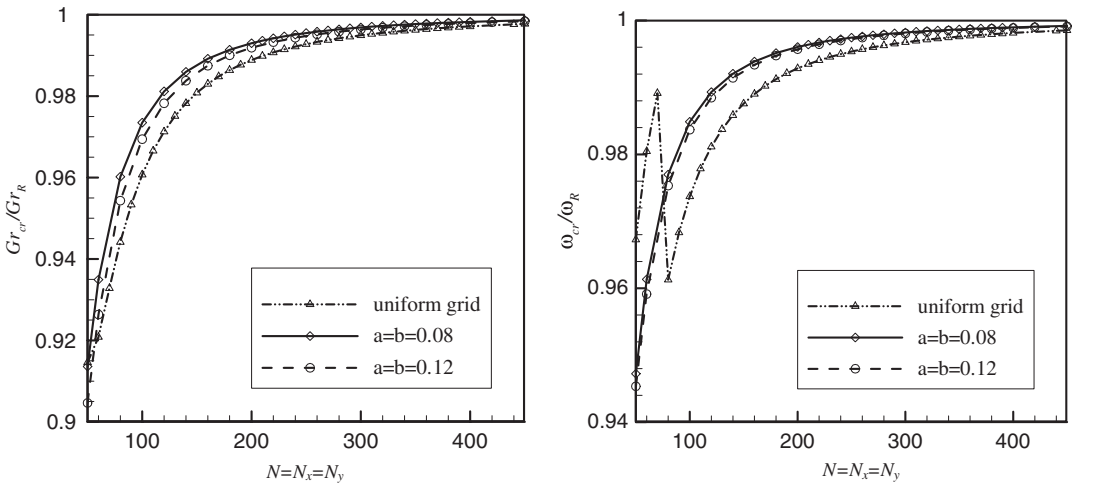

Figure 8. Effect of the stretching on the convergence of the critical Grashof number and critical frequency for problem 1. The subscript R stays for the Richardson extrapolation from the two finest uniform grids.

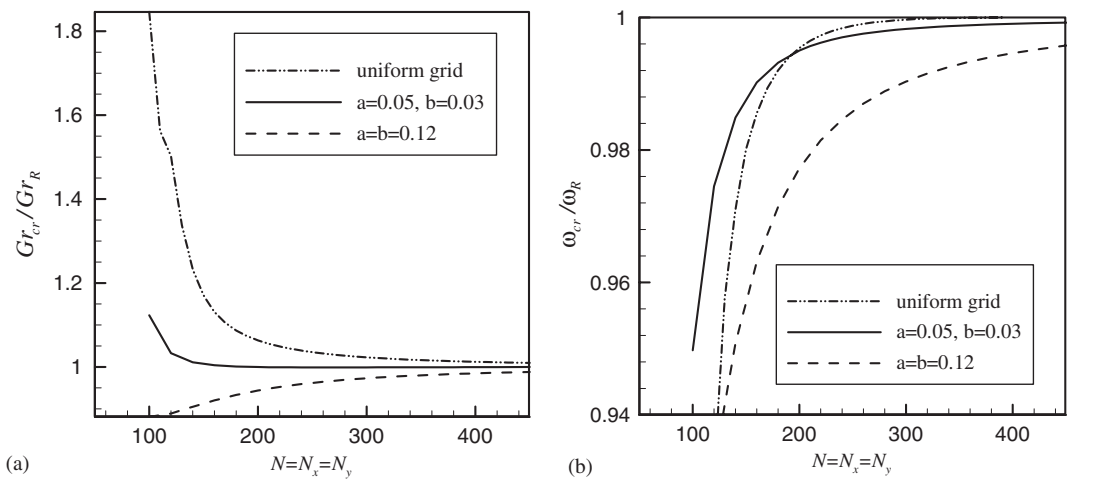

Figure 9. Effect of the stretching on the convergence of the critical Grashof number and critical frequency for problem 4. The subscript R stays for the Richardson extrapolation from the two finest uniform grids.

For the problem 4 (Figure 9) we observe much faster convergence of the critical Grashof number for the grid with the optimized parameters $a = 0.05$ and $b = 0.03$. However, the convergence of the critical frequency is fastest for the uniform grid, while the densely stretched grid with $a = b = 0.12$ shows a very slow convergence. This example shows that the stretching does not always speeds up the convergence and that it is not enough to check the effect of the stretching for only one characteristic parameter.

DOI: 10.1002/fld

4. CONCLUDING REMARKS

To summarize this study we emphasize once again the main conclusions made above. It is shown that the critical parameters converge very slowly with the grid refinement. Therefore, attempts to perform stability analysis on a coarse grid are expected to yield inaccurate and even wrong results. Our estimation for the finite volume method is that a quantitatively correct stability result can be expected starting from a grid having about 100 nodes in the shortest direction. This agrees with the convergence studies performed in References [24–26]. Apparently, for the higher-order methods the convergence can be achieved on coarser grids. However, higher-order schemes will affect the sparseness of the Jacobian matrix, which can make the present approach ineffective. A good candidate for further studies can be compact schemes described in Reference [33] and references therein.

We argued that using the uniform grids and the Richardson extrapolation, one can achieve a very good accuracy. It is shown also that the mesh stretching can speed up the convergence, as is usually expected. At the same time the example in Figure 9 shows that the stretching effect can be undesirable. One of the problems in using the stretching is the necessity to compare with an independent data, since otherwise it is impossible to conclude whether the accuracy of calculations is increased or decreased.

It is argued that the Arnoldi iterations can become faster if the iterative solvers are replaced by the direct ones. This conclusion, however, depends on the sparseness of the Jacobian matrix and can become wrong for higher-order methods for which the Jacobian matrix becomes significantly denser. In the case of the Newton iteration it was also found that a direct solver yields rather efficient and reliable computational process. The comparison with the approaches where exact and inexact Newton methods are combined with the iterative solvers is yet to be done. Apparently, the result of such a comparison will be problem dependent, as well as depend on a numerical method used for solution of the whole problem. It can be additionally argued here that approach using the direct solver is problem independent, and its CPU-time and memory consumption can be easily estimated.

APPENDIX A

Here we give several examples on the convergence of Newton iteration-based steady solver, Arnoldi eigensolver and the secant method used for calculation of the critical values. All the examples here, except of the last one, are made for the Problem 2. Note, that for more effective calculations the velocity and the time are scaled by $Gr^{1/2}$.

Convergence of the Newton iterations is illustrated in Table AI. The residuals are calculated as $\max_i [|\mathrm{d}x_i|/|x_i|]$, where x_i is a scalar variable and $\mathrm{d}x_i$ is the correction calculated at a current Newton iteration. For the critical value of Problem 2 calculated at 400×400 grid, we examine the convergence for initial guess interpolated from the solution on a coarser grid, as well as from solutions at the same grid but for smaller Grashof numbers. Linear interpolation between four grid points is used to map a solution from one grid to another one. The first three columns of Table AI show that when the data is transferred from a coarser grid the Newton method converges within three iterations. The convergence is slower when the initial guess is taken as a steady-state calculated for a different Grashof number. Apparently the Newton method can diverge if the initial guess is taken too far from solution. However, a graduate increase of the Grashof number allows us to calculate steady-states for all parameters needed, as well as far above the critical value.

DOI: 10.1002/fld

Table AI. Convergence of residuals of the Newton iterations. Calculation of the steady-state flow at $Gr = 2.9 \times 10^6$ for Problem 2 using grid 400×400.

Iteration	From grid 100×100 $Gr = 2.9 \times 10^6$	From grid 200×200 $Gr = 2.9 \times 10^6$	From grid 300×300 $Gr = 2.9 \times 10^6$	From grid 400×400 $Gr = 2.0 \times 10^6$	From grid 400×400 $Gr = 10^6$
1	0.6715	0.6341	0.6338	0.8399×10^{-3}	0.1986×10^{-2}
2	0.4260×10^{-4}	0.6341×10^{-5}	0.6338×10^{-5}	0.2417×10^{-3}	0.1194×10^{-2}
3	0.7675×10^{-8}	0.2111×10^{-9}	0.2378×10^{-9}	0.9965×10^{-6}	0.8729×10^{-4}
4				0.1329×10^{-8}	0.1085×10^{-6}
5					0.4457×10^{-10}

Table AII. Convergence of the secant method iterations used for calculation of the critical Grashof number. Problem 2, grid 400×400.

Iteration	Gr	max[Real(λ)]	Gr	max[Real(λ)]	Gr	max[Real(λ)]
0	2×10^6	−0.10416	2.4×10^6	−0.056010	2.8×10^6	−0.010912
1	2.002×10^6	−0.10345	2 402 400	−0.055713	2 802 800	−0.010627
2	4 896 668	+0.12144	2 853 081	-0.5554×10^{-2}	2 909 544	-0.7224×10^{-5}
3	3 337 415	+0.037301	2 909 528	-0.8937×10^{-5}	2 909 619	-0.4498×10^{-7}
4	2 646 144	−0.027247	2 909 534	-0.8212×10^{-5}		
5	2 937 948	0.027250	2 909 619	-0.4968×10^{-7}		
6	2 911 418	0.1742×10^{-3}				
7	2 909 607	-0.1299×10^{-5}				
8	2 909 619	-0.1772×10^{-7}				

Table AII shows the convergence of the secant method for three different starting values of the Grashof number. It is seen that the closer is the starting value to the critical one, i.e. $Gr_{cr} = 2.9096 \times 10^6$ in the example considered, the smaller is the number of secant iterations needed to calculate the critical value. The critical values shown in Table AII are calculated to within five correct decimal digits, for which we needed nine iterations starting from $Gr = 2.0 \times 10^6$, six iterations starting from $Gr = 2.4 \times 10^6$, and four iterations starting from $Gr = 2.8 \times 10^6$. Apparently, if the starting value is chosen too far from the critical one the number of secant iterations can be even larger. The whole secant iteration process can diverge if wrong leading eigenvalue is selected at the starting iteration. In the convergence studies reported above the starting value can be chosen very close to the critical one after the convergence to within 2 decimal digits is achieved. Thus 4–6 secant iterations are needed to calculate the critical values, as described above. When the parametric stability studies are performed (see, e.g. References [9, 10, 14, 15]), the critical values vary continuously with variation of other parameters, which allows one to choose the starting values close to the critical ones. Thus, at the continuous parts of the neutral stability curves 4–6 secant iterations usually are sufficient. Larger number of iterations is needed near the points corresponding to the bifurcations with higher co-dimension, where different leading eigenvalues cross the real axis at close values of governing parameters.

DOI: 10.1002/fld

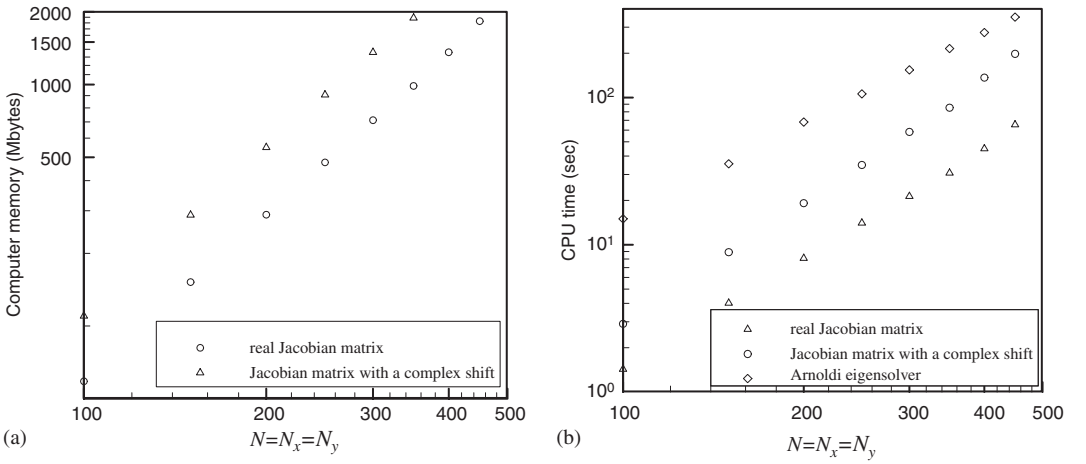

Figure AI. Computer memory and CPU time consumed for **LU**-decomposition of the real Jacobian matrix needed for the Newton iteration, the Jacobian matrix with complex shift needed for the shift-and-invert Arnoldi iteration and the Arnoldi eigensolver. The estimation is done for Problem 2.

The computer memory and CPU time required for the **LU**-decomposition (using the MUMPS code) of the real Jacobian matrix needed for the Newton iteration and the same Jacobian matrix with a complex shift used for the shift-and invert Arnoldi iteration together with the CPU time consumed by the Arnoldi eigensolvers (using the ARPACK code) are shown in Figure AI. The memory needed for the **LU**-decomposition scales as $N^{2.3}$, where N is the number of grid points in one spatial direction. The CPU times have no such a clear scaling. Their change can be estimated as $N^{2.6}$, N^3, N^2, for the real Jacobian, Jacobian with a complex shift and Arnoldi eigensolvers, respectively. For all the problems considered the number of Arnoldi iterations varied between 6000 and 7000 and was almost independent on grid refinement.

Comparison with other numerical approaches to direct steady-state calculations and stability analysis should be done for the same physical problem, same numerical method applied to the initial problem, and preferably for the same or similar computers. Such a comparison is beyond the scope of the present study. Here we can report a comparison with the results of Reference [25], where problem 7 was solved by the finite element method in the Galerkin least squares formulation. The finest grid reported was 256×688. This leads to 708 292 degrees of freedom, which is exactly the same as for the 256×688 grid finite volume method used in the present study. The time needed for four Newton iterations, which in Reference [25] and here was enough for the convergence, was reported in Reference [25] to be 3.5 h with the use of 160 processors. The time consumed in the present work on a single Itanium-2 processor was 192 s. The time needed for one run of the eigenvalues calculation was reported in Reference [25] to be 4 h on 128 processors for an Arnoldi space of size 150 and 27 leading eigenvalues converged. For the same parameters of the Arnoldi method the present approach consumed 750 s for Arnoldi iterations and 140 s for the **LU**-decomposition on the single Itanium-2 processor.

ACKNOWLEDGEMENTS

This study was supported by the German-Israeli Foundation, Grant No. 1-794-145.10/2004.

DOI: 10.1002/fld

REFERENCES

1. Botella O, Peyret R. Benchmark spectral results on the lid-driven cavity flow. *Computers and Fluids* 1998; **27**:421–433.
2. Le Quéré P. Accurate solutions to the square thermally driven cavity at high Rayleigh number. *Computers and Fluids* 1991; **20**:29–41.
3. de Vahl Davis G, Jones IP. Natural convection in a square cavity: a comparison exercise. *International Journal for Numerical Methods in Fluids* 1983; **3**:227–264.
4. Le Quéré P. Contribution to GAMM workshop with a pseudo-spectral algorithm on a staggered grid. In *Proceedings of the GAMM Workshop on Numerical Simulation of Oscillatory Convection in Low Prandtl Number Fluids*, Roux B (ed.). Notes on Numerical Fluid Mechanics, vol. 27. Vieweg Braunschweig, 1989; 227–236.
5. Pulicani JP, Crespo del Arco A, Randriamampianina A, Bontoux P, Peyret R. 1989, Spectral simulations of oscillatory convection at low Prandtl number. *International Journal for Numerical Methods in Fluids* 1989; **10**:481–517.
6. Roux B (ed.). *Proceedings of the GAMM Workshop on Numerical Solution of Oscillatory Convection in Low Prandtl Number Fluids*, Marseille, 1988. Notes on Numerical Fluid Mechanics, vol. 27. Vieweg Braunschweig, 1989.
7. Xin S, Le Quéré P. An extended Chebyshev pseudo-spectral benchmark for the 8:1 differentially heated cavity. *International Journal for Numerical Methods in Fluids* 2002; **40**:981–998.
8. Christon MA, Gresho PM, Sutton SB. Computational predictability of time-dependent natural convection flows in enclosures (including benchmark solution). *International Journal for Numerical Methods in Fluids* 2002; **40**:953–980.
9. Gelfgat AY, Bar-Yoseph PZ, Yarin AL. On oscillatory instability of convective flows at low Prandtl number. *Journal of Fluids Engineering* 1997; **119**:823–830.
10. Gelfgat AY, Bar-Yoseph PZ, Yarin AL. Stability of multiple steady states of convection in laterally heated cavities. *Journal of Fluid Mechanics* 1999; **388**:315–334.
11. Gelfgat AY. Stability and slightly supercritical oscillatory regimes of natural convection in a 8:1 cavity: solution of benchmark problem by a global Galerkin method. *International Journal for Numerical Methods in Fluids* 2004; **44**:135–146.
12. Gelfgat AY. Two- and three-dimensional instabilities of confined flows: numerical study by a global Galerkin method. *Computational Fluid Dynamics Journal* 2001; **9**:437–448.
13. Gelfgat AY. Implementation of arbitrary inner product in global Galerkin method for incompressible Navier–Stokes equation. *Journal of Computational Physics* 2005; **211**:513–530.
14. Gelfgat AY, Rubinov A, Bar-Yoseph PZ, Solan A. numerical study of three-dimensional instabilities in a hydrodynamic model of Czochralski growth. *Journal of Crystal Growth* 2005; **275**:e7–e13.
15. Gelfgat AY, Rubinov A, Bar-Yoseph PZ, Solan A. On the three-dimensional instability of thermocapillary convection in arbitrary heating floating zones in microgravity environment. *Fluid Dynamics and Material Processing* 2005; **1**:21–31.
16. Johnson RW, McHugh PR, Knoll DA. High-order scheme implementation using Newton–Krylov solution methods. *Numerical Heat Transfer* 1997; **31**:295–312.
17. Fokkema DR, Sleijpen GLG, van der Vorst HA. Accelerated inexact Newton schemes for large systems of nonlinear equations. *SIAM Journal on Scientific Computing* 1998; **19**:657–674.
18. Qin N, Ludlow D, Shaw ST. A matrix-free preconditioned Newton/GMRES method for unsteady Navier–Stokes solutions. *International Journal for Numerical Methods in Fluids* 2000; **33**:223–248.
19. Knoll DA, Keyes DE. Jacobian-free Newton–Krylov methods: a survey of approaches and applications. *Journal of Computational Physics* 2004; **193**:357–397.
20. Edwards WS, Tuckerman LS, Friesner RA, Sorensen DC. Krylov methods for the incompressible Navier–Stokes equations. *Journal of Computational Physics* 1994; **110**:82–102.
21. Gadoin E, Le Quéré P, Daube O. A general methodology for investigating flow instabilities in complex geometries: application to natural convection in enclosures. *International Journal for Numerical Methods in Fluids* 2001; **37**:175–208.
22. Hwang FN, Cai XC. A parallel additive Scwartz preconditioned inexact Newton algorithm for incompressible Navier–Stokes equations. *Journal of Computational Physics* 2005; **204**:666–691.
23. Sanchez J, Marques F, Lopez JM. A continuation and bifurcation technique for Navier–Stokes equations. *Journal of Computational Physics* 2002; **180**:82–102.

DOI: 10.1002/fld

24. Lechoucq RB, Salinger AG. Large-scale eigenvalue calculations for stability analysis of steady flows on massively parallel computers. *International Journal for Numerical Methods in Fluids* 2001; **36**:309–327.
25. Salinger AG, Lechoucq RB, Pawlowski RP, Shadid JN. Computational bifurcation and stability studies of the 8:1 thermal cavity problem. *International Journal for Numerical Methods in Fluids* 2002; **40**:1059–1073.
26. Burroughs EA, Romero LA, Lechouq RB, Salinger AG. Linear stability of flow in a differentially heated cavity via large-scale eigenvalue calculations. *International Journal of Numerical Methods for Heat and Fluid Flow* 2004; **14**:803–822.
27. van der Vorst HA. *Iterative Krylov Methods for Large Linear Systems*. Cambridge University Press: Cambridge, 2003.
28. Onur O, Eyi S. Effects of the Jacobian evaluation on Newton's solution of the Euler equations. *International Journal for Numerical Methods in Fluids* 2005; **49**:211–231.
29. Lechouq RB, Sorensen DC, Yang C. *ARPACK Users' Guide*: *Solution of Large Scale Eigenvalue Problems with Implicitly Restarted Arnoldi Methods*. SIAM: Philadelphia, 1998.
30. Patankar SV. *Numerical Heat Transfer and Fluid Flow*. Hemisphere/McGraw-Hill: New York, 1980.
31. Xu J, Zebib A. Oscillatory two- and three-dimensional thermocapillary convection. *Journal of Fluid Mechanics* 1998; **364**:187–209.
32. Cliffe KA, Tavener SJ. Marangoni-Bénard with a deformable free surface. *Journal of Computational Physics* 1998; **145**:193–227.
33. Pereira JMC, Kobayashi MH, Pereira JCF. A fourth-order accurate finite-volume compact method for the incompressible Navier–Stokes solutions. *Journal of Computational Physics* 2001; **167**:217–243.

DOI: 10.1002/fld